Raman spectroscopic study of the phase transitions and pseudospin phonon coupling in sodium ammonium sulphate dihydrate

J. Agostinho Moreira,* A. Almeida, M. R. Chaves, M. L. Santos, and P. P. Alferes
Departamento de Física da Faculdade de Ciências, IFIMUP, Universidade do Porto, Rua do Campo Alegre 687, 4169-007 Porto, Portugal

I. Gregora
Institute of Physics, Academy of Sciences of the Czech Republic, Na Slovance 2, 18221 Prague 8, Czech Republic
(Received 19 April 2007; revised manuscript received 5 July 2007; published 5 November 2007)

This work reports a detailed study of the temperature dependence of the lattice dynamics of single crystal sodium ammonium sulphate dihydrate (SASD) obtained from polarized Raman scattering. The phase transitions in SASD are marked by the appearance of new weak bands and anomalies in the temperature dependence of wave number and damping factor of several lattice and internal modes. The temperature dependence of the symmetric bending modes of ammonium ion as well as the abrupt shift of wave number of some lattice and internal modes related to the molecular units point to a proton ordering mechanism associated with the paraelectric-ferroelectric phase transition. The anomalies, which have been detected in the temperature dependence of the wave number and of the damping coefficient of some external and internal modes, are well described by a theoretical model that takes into account the coupling between pseudospins and phonons.

DOI: 10.1103/PhysRevB.76.174102 PACS number(s): 77.84.−s, 63.20.−e, 78.30.−j, 64.60.−i

I. INTRODUCTION

A structural phase transition is usually considered to be either of the displacive or order-disorder nature, depending on the microscopic mechanism associated. A displacive structural phase transition is characterized by the existence of a critical optical soft mode, associated with instability of a lattice mode.[1] An order-disorder phase transition involves a critical slowing down of a relaxation mode, whose frequency typically lies in the microwave region.[2] This relaxation mode is related to the dynamical hopping of disordered atoms or molecular groups among several close potential minima sites in the unit cell.

During the last few years, experimental results have shown that a displacive feature often exists even in order-disorder phase transitions. In fact, due to the coupling between the different structural units, the ordering of atoms or molecular groups alters the potential and, as a consequence, deformations of polyatomic groups occur. This is the case of KDP, where the ordering of protons in hydrogen bonds is not sufficient to explain its ferroelectric properties.[3] It was shown that the motion of heavy atoms coupled to protons must be taken into account to obtain a more realistic description of its phase transition. Other systems display coupling between the ordering mechanism and deformation of molecular groups. Triglycinium sulphate undergoes an order-disorder phase transition related to the sulphate ions. A strong coupling between the pseudospin, associated with the sulphate ions, and lattice vibrations was found in this compound.[4] Another example is the ferroelectric phase transition in glycinium phosphite, where a strong coupling between proton pseudospins and normal modes was found together with deformations of the molecular units.[5]

Similar to the previous three cases, a significant number of ferroelectric materials containing tetrahedral ions, such as SO_4^{2-}, NH_4^+, PO_4^{3-}, and AsO_4^{3-}, exhibit pseudospin phonon coupling, which plays an important role in the microscopic mechanism related to the phase transitions. We find that sodium ammonium sulphate dihydrate is a good example among these compounds.

Sodium ammonium sulphate dihydrate (SASD) is an ammonium sulphate based compound, with chemical formula $NaNH_4SO_4 \cdot 2H_2O$. SASD exhibits interesting physical properties at low temperatures. This compound presents a variety of chemical bonds, including hydrogen bonds, which may play an important role in its polar properties at low temperatures.

At room temperature, SASD is orthorhombic with the spatial group $P2_12_12_1$.[6] The primitive cell has four molecules.[6] The sulphate ions have the usual tetrahedral coordination, with a mean S-O distance of about 1.47 Å, and angles with small deviations from the tetrahedral values, while the coordination polyhedron of the NH_4^+ ions is very irregular. The crystalline structure of SASD is formed by chains of sodium-oxygen octahedra, NaO_6, approximately aligned along the *c* axis, sharing three O atoms on a face and interspaced by chains of NH_4^+-SO_4^{2-}-NH_4^+ ions, linked together by hydrogen bonds (see Fig. 1 of Ref. 7). The two types of chains share one oxygen atom of the SO_4^{2-} anion. The two water molecules belong to the NaO_6 polyhedron and make additional hydrogen bonds between Na and NH_4^+ polyhedra.

The dielectric behavior and critical temperatures of SASD strongly depend on the preparation method.[8] Single crystals of SASD prepared by slow evaporation of an aqueous solution with equimolar ratio of Na_2SO_4 and $(NH_4)_2SO_4$ at room temperature are known to be ferroelectric below T_{c1} = 101 K.[8] The crystals containing excess of $(NH_4)_2SO_4$ exhibit a larger temperature interval between the two dielectric peak anomalies. On cooling, the dielectric constant, measured along the *c* axis at 1 kHz, displays steplike anomalies

at $T_{c1}=101$ K and at $T_{c2}=92$ K, accompanied by thermal hysteresis of about 2 K.[8] The maximum value of the dielectric constant is 17, near T_{c1}. The features displayed by the dielectric constant suggest the existence of two phase transitions both of first order. The spontaneous polarization, calculated by integration of the pyroelectric current, measured along the c axis on a cooling run displays a sudden increase at T_{c1} and another step at $T_{c2}=92$ K.[8] The value of the spontaneous polarization at 80 K is about 7 nC/cm^2, a rather low value for a typical ferroelectric material. Although it had been indicated that the space group of the structure of the ferroelectric phase is $P2_1$, no structural data have yet been published, as far as we know.

The main feature of the dynamics of SASD is the rapid rotation of the SO_4^{2-} anions around one of the tetrahedral axes and their distortion below $T_{c1}=101$ K.[9] The nonequivalence of the two nearest anion rotations leads to the identification of two sublattices of SO_4^{2-} anions in the crystal. In the paraelectric phase, these two sublattices of SO_4^{2-} (I) and SO_4^{2-} (II) anions are equivalent, but oppositely oriented, so that the total polarization is equal to zero. Below $T_{c1}=101$ K, due to the different angles at which the sulphate anions freeze their reorientations, the symmetry of the crystal lowers and a nonzero polarization appears along the c axis. This mechanism has been viewed as resulting from an order-disorder process of the sulphate ion (Ref. 10) and described on the basis of the Mitsui model (Refs. 10–12). The Mitsui model requires two types of active molecular groups in a two-lattice system. In SASD, this two-lattice system would be formed by the SO_4^{2-} (I) and SO_4^{2-} (II) anions.

The wealth of chemical bonds present in the crystal of SASD, along with the existence of two dielectric anomalies, suggests that one may likely have to go beyond the simple approximation of an order-disorder model in order to fully understand the mechanism of the phase transition in SASD. These include other order-disorder processes, such as the ordering of hydrogen bonds, together with additional deformations of the sulphate ions, as well as coupling between the pseudospins and lattice modes.

Microscopic studies on SASD are rather scarce. A recent paper concerning an infrared reflectivity study of the phase transition in SASD confirms the existence of the complex mechanism associated with the phase transitions at low temperatures and reveals a strong coupling between pseudospins and normal modes in SASD.[7] However, no quantitative analysis of the experimental data supports the latter conclusion. Raman scattering spectroscopy has been revealed to be a powerful technique in the study of lattice dynamics and coupling phenomena, especially the pseudospins and normal mode coupling, in a great variety of compounds.[4,5] To the best of our knowledge, only Fawcett *et al.* have published a polarized Raman scattering study of SASD, performed between room temperature and 87 K.[13,14] Hence, this study does not provide a detailed and quantitative lattice dynamics analysis of the low temperature phases of SASD.

In this work, we report a detailed experimental study on sodium ammonium sulphate dihydrate by polarized Raman spectroscopy in the temperature range 20–300 K. The polarized Raman spectra allow us to follow the temperature behavior of the vibrational parameters through the two low temperature structural phase transitions in order to clarify the mechanisms underlying the critical behavior in SASD.

II. EXPERIMENTAL DETAILS

The colorless single crystals of SASD used in our Raman scattering study have been obtained by slow controlled evaporation at 40 °C from the aqueous solution of the constituents with equimolar ratio of Na_2SO_4 and $(NH_4)_2SO_4$.

The samples used have the form of oriented and optically polished parallelepipeds ($3\times4\times5$ cm^3). As SASD exhibits orthorhombic structure at room temperature, the faces of the samples were cut normal to $X\|a$, $Y\|b$, and $Z\|c$ axis. The samples were placed in a closed-cycle helium cryostat (10–300 K temperature range) with a temperature stability of about ±0.2 K. The temperature homogeneity in the samples was achieved with a copper mask setup. The temperature of the sample was estimated to differ by less than 1 K from the temperature measured with a silicon diode attached to the sample holder.

The polarized Raman spectra of SASD have been measured in the right-angle scattering geometry, on cooling runs. At room temperature, we recorded spectra in the six different scattering geometries. The temperature dependence of the vibrational parameters was mainly obtained by studying the spectra in the $y(XX)z$, $x(YY)z$, and $x(ZZ)y$ configurations (Porto's notation, referring to the Cartesian system defined above). The 514.5 nm polarized line of an Ar^+ laser Coherent INOVA 90 was used for excitation, with an incident power of about 50 mW impinging on the sample. The scattered light was analyzed using a T64000 Jobin-Yvon spectrometer, operating in triple subtractive mode and equipped with liquid nitrogen cooled charge coupled device and photon-counting device. Identical conditions were maintained for all scattering measurements. The spectral slit width was about 1.5 cm^{-1}.

The Raman spectra of SASD were fitted with a sum of independent damped harmonic oscillators, according to the general formula

$$I(\omega,T)=[1+n(\omega,T)]\sum_{j=1}^{N}A_{oj}\frac{\omega\Omega_{oj}^2\Gamma_{oj}}{(\Omega_{oj}^2-\omega^2)^2+\omega^2\Gamma_{oj}^2}. \quad (1)$$

Here, $n(\omega,T)$ is the Bose-Einstein factor, and A_{oj}, Ω_{oj}, and Γ_{oj} are the strength, wave number, and damping coefficient of the jth oscillator, respectively. Below 230 cm^{-1}, for the purpose of the fit, the Rayleigh scattering wing at the lowest frequencies was modeled by a fixed Gaussian component with a half-width of about 4 cm^{-1} in the whole temperature interval. No Debye mode was considered in the fit procedure of the low frequency spectra, as no relaxational mode was detected.

III. EXPERIMENTAL RESULTS AND DISCUSSION

In this section, we describe the Raman spectra obtained in the 20–3800 cm^{-1} wave number range. Figure 1 shows the Raman spectra corresponding to the six components of the polarizability tensor of SASD, obtained at 300 K.

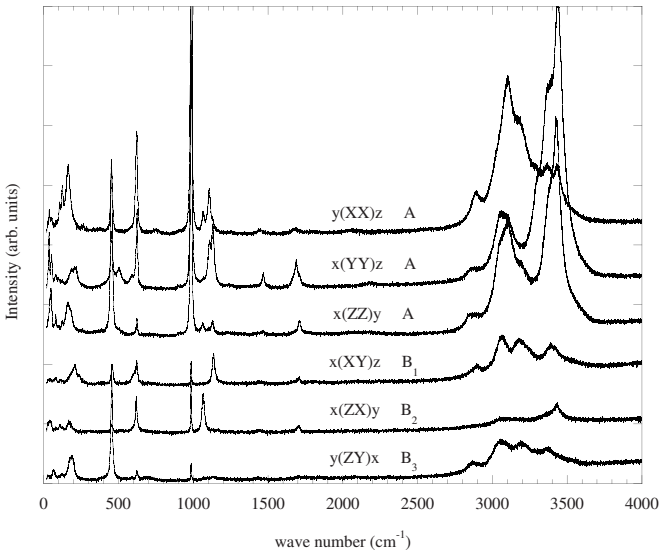

FIG. 1. Overall Raman spectra of SASD at room temperature for six scattering geometries. The spectra are vertically shifted by comparison.

According to x-ray data at room temperature, the primitive cell contains 4 formula units, i.e., 68 atoms, and the factor group is isomorphic to the point group D_2. In the paraelectric phase, all atoms occupy sites of C_1 symmetry. The dynamics of the crystal lattice is described in terms of 201 optical and 3 acoustical modes. As follows from factor group analysis, in the paraelectric phase, we expect 51 A, 50 B_1, 50 B_2, and 50 B_3 first-order Raman lines. All modes are Raman active and the B_1, B_2, and B_3 modes are also infrared active. Due to the polar nature of B_1, B_2, and B_3 modes, their frequencies, measured in the right-angle scattering geometries, may be influenced by directional dispersion and they correspond, in general, to mixed modes (neither pure TO nor pure LO) depending on the direction of the scattering wave vector with respect to the reference system. The B_1 modes of mixed TO-LO character are observed in the $x(YX)z$ geometry, whereas pure B_1(TO) modes would be observed in the $x(ZY)z$ geometry.

Considering the SO_4^{2-}, NH_4^+, and H_2O polyatomic groups as rigid units and taking into account that the Na atom can only have translational modes, we obtain 15 A +14 B_1+14 B_2+14 B_3 and 12 A+12 B_1+12 B_2+12 B_3 external translations and libration modes, respectively.

A. Mode assignment at room temperature

The identification of some of the normal modes observed in the Raman spectra of SASD was based on the relevant information referred to in the literature (Refs. 13 and 14) and in the comparative study of the Raman and infrared reflectivity spectra (Ref. 7) as well as the comparative analysis of the Raman spectra of SASD and lithium ammonium sulphate (LAS) or ammonium sulphate.[15,16] In general, we found good agreement between our data and the results previously reported.[13,14]

In the following two sections, we propose a mode assignment of the bands observed in our Raman spectra, recorded at 300 K, starting with the problem of identifying the lattice modes.

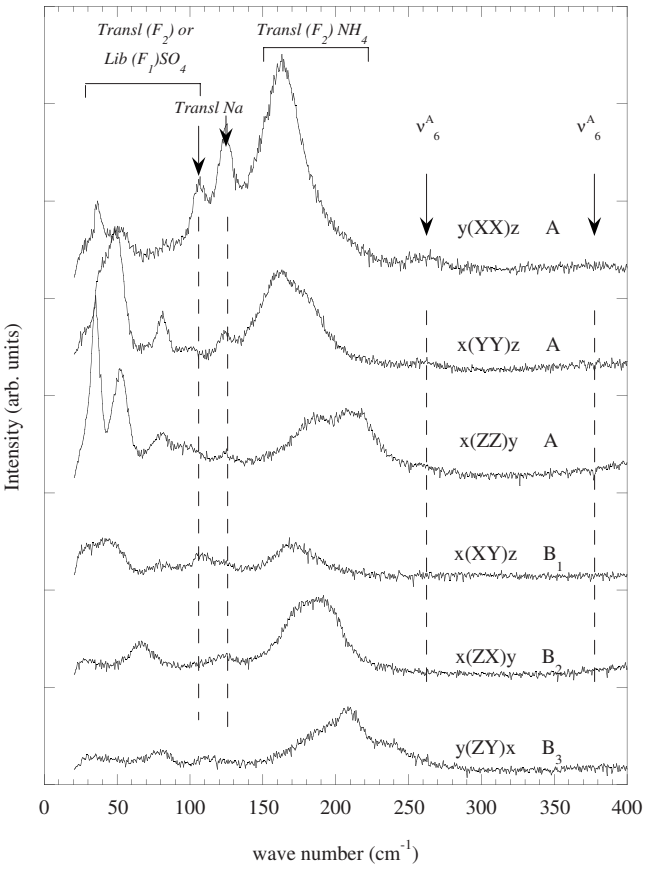

FIG. 2. Raman spectra of SASD recorded at room temperature for six scattering geometries in the wave number range of external modes. The spectra are vertically shifted by comparison.

1. Lattice modes

Figure 2 shows the Raman spectra of SASD in the region of lattice modes in the six different scattering geometries.

Using a fitting procedure, we have detected nine lattice modes at room temperature, with wave number below 350 cm^{-1}. These bands result from translational and librational modes of the various units, including the Na-O modes. As was referred to above, we expected to find 27 A, 26 B_1, 26 B_2, and 26 B_3 optical lattice modes. Mode mixing, partial or total overlap of the lattice bands, or very weak mode strength may be at the origin of this discrepancy.

A detailed identification of the low wave number bands is not possible, but some general assignments are possible. For assignment purposes, we have taken into account the relevant information regarding frequencies of the lattice modes associated with sulphate and ammonium ions in several ammonium sulphate based crystals. Although the frequencies of the lattice modes associated with translations and rotations of the molecular units are strongly influenced by the crystal environment, it was found, in many ammonium sulphate based crystals, that librations and translations of the sulphate ion are usually located in the 70–130 cm^{-1} wave number range, and external modes associated with the ammonium

TABLE I. Symmetry and wave number (in cm^{-1}) of the vibrational modes in the free molecular units of SASD.

		C_{2v}			
		ν_1	ν_2		ν_3
Free molecule	H_2O	3657 cm^{-1}	1595 cm^{-1}		3756 cm^{-1}
Symmetry		A_1	B_1		A_1
		T_d			
		ν_1	ν_2	ν_3	ν_4
Free ion	NH_4^+	3033 cm^{-1}	1685 cm^{-1}	3134 cm^{-1}	1397 cm^{-1}
	SO_4^{2-}	981 cm^{-1}	451 cm^{-1}	1104 cm^{-1}	613 cm^{-1}
Symmetry		A_1	E	F_2	F_2

ion are located between 165 and 228 cm^{-1} and at 394 cm^{-1}.[16] The rotational degrees of freedom of the molecular groups may give rise, in a crystal, to librational modes. In the case of tetrahedral ions, these modes are designated by ν_6 and can be combined with bending modes ν_2 and ν_4 to give rise to combinational modes $\nu_6+\nu_2$ and $\nu_6+\nu_4$.[17] Acharya and Naraynan detected in the infrared spectra of SASD recorded at room temperature two ν_6 modes of the ammonium ion with wave number 255 and 310 cm^{-1}, respectively, along with a combinational mode $\nu_6+\nu_2$ at 2070 cm^{-1}.[18] However, Fawcett *et al.* assigned the broad band located at 385 cm^{-1} in the Raman spectra as a ν_6 mode of the ammonium ion.[13] From our Raman spectra (see Fig. 2), we are able to detect two broad and weak bands, located at 261 and at 385 cm^{-1} that we assign to the ν_6^A mode of the ammonium ion.

The detailed assignment of the Na translation modes was not possible from the available data.

2. Internal modes

The internal mode frequencies of the SO_4^{2-} and NH_4^+ ions can be readily assigned by comparison with the free ion frequencies.

The free sulphate and ammonium ions, with T_d symmetry, have four normal modes, all Raman active: the nondegenerate and totally symmetrical stretching mode ν_1, the doubly degenerate bending mode ν_2, the triply degenerate stretching mode ν_3, and the triply degenerate bending mode ν_4.[19]

The free water molecule, with symmetry C_{2v}, possesses three internal vibrations, namely, the symmetric stretching mode ν_1, the antisymmetric stretching mode ν_3, and the bending mode ν_2. Table I summarizes the numerical values reported for the wave number of internal modes associated with the sulphate ion, the ammonium ion, as well as the water molecule in solid hydrates.[20]

In many compounds containing tetrahedral ions or water molecules, the identity of these units is maintained. Frequently, the influence of a less symmetrical crystallographic environment lifts the degeneracy of the modes. Since the site symmetry of all units is C_1 (i.e., identity), each characteristic vibration of free molecular units transforms into a component in all four symmetry types (A, B_1, B_2, and B_3) of the factor group. Therefore, we expect to observe, in each first-order Raman spectra, nine bands associated with the vibrations of both sulphate and ammonium ions and six bands concerning the internal vibrations of the water molecule in each symmetry species. However, as the primitive cell has 4 formula units, we should expect, in the first-order Raman spectra, four times as many internal modes, corresponding to different normal modes combined from the vibrations of individual molecular units. This effect is usually known as Davydov splitting.[21]

Let us consider the internal modes of the SO_4^{2-} ion. Figure 3 shows the Raman spectra of SASD in the 400–1200 cm^{-1} range in all scattering geometries. The fully symmetric stretching mode ν_1^S is well observed at 986 cm^{-1} in all totally symmetric species, giving rise to strong bands in the A spectra of the paraelectric phase, as can be seen in Fig. 3. The weak and broad band, observed at 906 cm^{-1} in the A spectra, has origin in the first overtone of the ν_2^S of the sulphate anion. Among the two components expected from symmetry considerations for the ν_2^S bending mode, only one component is visible in the $A(zz)$, $B_1(xy)$, $B_2(yz)$, and $B_3(zx)$ Raman spectra; this band is located between 453 and 457 cm^{-1}, depending on the respective scattering geometry (see Fig. 3). However, in the $A(xx,yy)$ Raman spectra, we have two components for obtaining a good fit to the band observed between 430 and 480 cm^{-1}; the two components of the resolved band are located at 452 and 460 cm^{-1}, respectively. We cannot detect, in either spectra, the three bands associated with the bending modes ν_4^S; in fact, we have taken only two components for fitting the band located between 610 and 640 cm^{-1} in the $A(xx,yy)$, $B_1(xy)$ and $B_2(yz)$ Raman spectra, while the $A(zz)$ and B_3 spectra have been fitted very well to the band with just one component located at 624 cm^{-1}. The two components associated with the ν_4^S mode are located at about 617 and 625 cm^{-1}, respectively. The broad bands observed at 506 and 583–587 cm^{-1} correspond to the librational modes of the water molecule. The triplet, whose components are located near 1065, 1106, and 1135 cm^{-1}, is associated with the triply degenerate antisymmetric stretching mode ν_3^S of the free ion. The three components are visible in all symmetry species. This result indicates that the sulphate ion loses its tetrahedral symmetry. As was referred to above, we expected to find 12 vibration

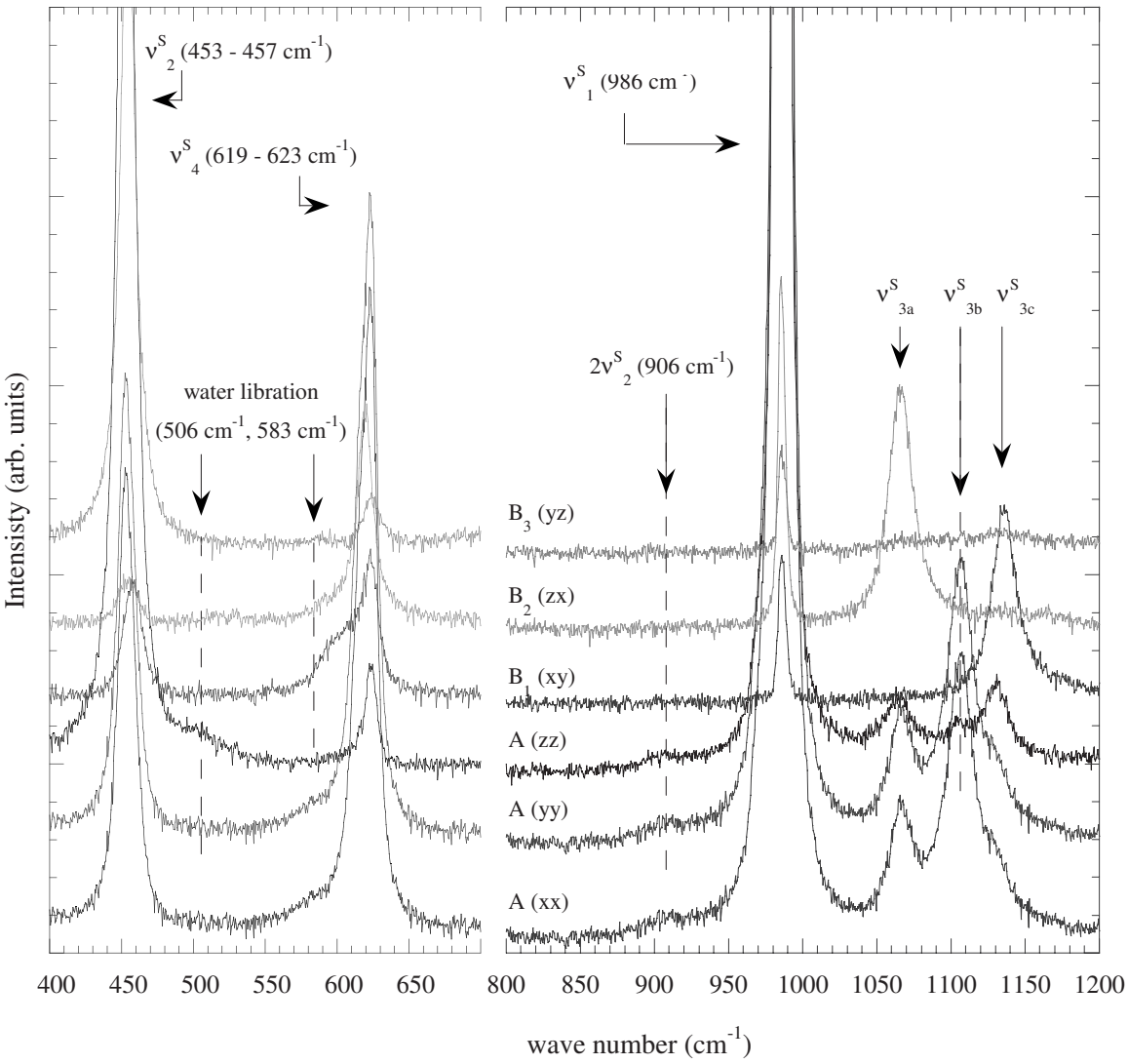

FIG. 3. Raman spectra of SASD recorded at room temperature for six scattering geometries in the wave number range of internal vibration of the sulphate ion. The spectra are vertically shifted by comparison.

bands originating from both ν_3^S and ν_4^S modes of the free ion. However, we could detect only three bands or less. This discrepancy may be due to a rather small Davydov splitting.

Let us now turn to the assignment of the internal vibrations of the ammonium ion. Figure 4 shows the Raman spectra of SASD in the wave number range between 1400 and 3700 cm^{-1}. In the $A(xx,yy,zz)$ Raman spectra, we observe two bands in the 1400–1500 cm^{-1} wave number range, whereas in the B_1 and B_2 Raman spectra, only one band is observed. These bands are associated with the asymmetric bending modes ν_4^A of the ammonium ion. In the spectral range between 1600 and 1800 cm^{-1}, we can clearly observe two bands in the A and B_1 spectra, corresponding to the asymmetric bending mode ν_2^A of the ammonium ion, whereas in the B_2 spectrum, we only observe one band at 1705 cm^{-1}, and in the B_3 spectrum, a very weak band is observed centered at 1700 cm^{-1}.

We expect to observe the stretching modes of the ammonium ion in the spectral range 2800–3300 cm^{-1}. The region of the ν_1^A and ν_3^A modes is more difficult to analyze due to the Fermi resonance with the overtones $2\nu_4^A$ and $2\nu_2^A$ and the mode combination $\nu_4^A+\nu_2^A$ as well as due to the presence of bands arising from the stretching modes of the water molecule. For purpose of assignment of the bands observed in this spectral range, we compared the obtained Raman spectra of SASD with those of LAS.[15] As LAS is a nonhydrated crystal, the high frequency vibrational spectra only exhibit ammonium internal modes. Figure 5 shows the Raman spectra of SASD and LAS, taken at room temperature, in the $x(ZZ)y$ scattering geometry. Taking into account the values referred to by Fawcett *et al.* and by Yuzyuk *et al.* (Refs. 14 and 15), we assign the broad bands located between 2800 and 2940 cm^{-1} to the $2\nu_4^A$ mode. The triplet observed between 3050 and 3300 cm^{-1} is assigned to ν_3^A, and the single band located at 3048 cm^{-1} is assigned to ν_1^A. The band located at 3362 cm^{-1} arises from the overlap of the $2\nu_2^A$ and the stretching mode of the water molecule, while the band located at 3449 cm^{-1} is associated with the stretching mode of the water molecule. The relatively intense bands, associated with the overtones and mode combination, give clear evi-

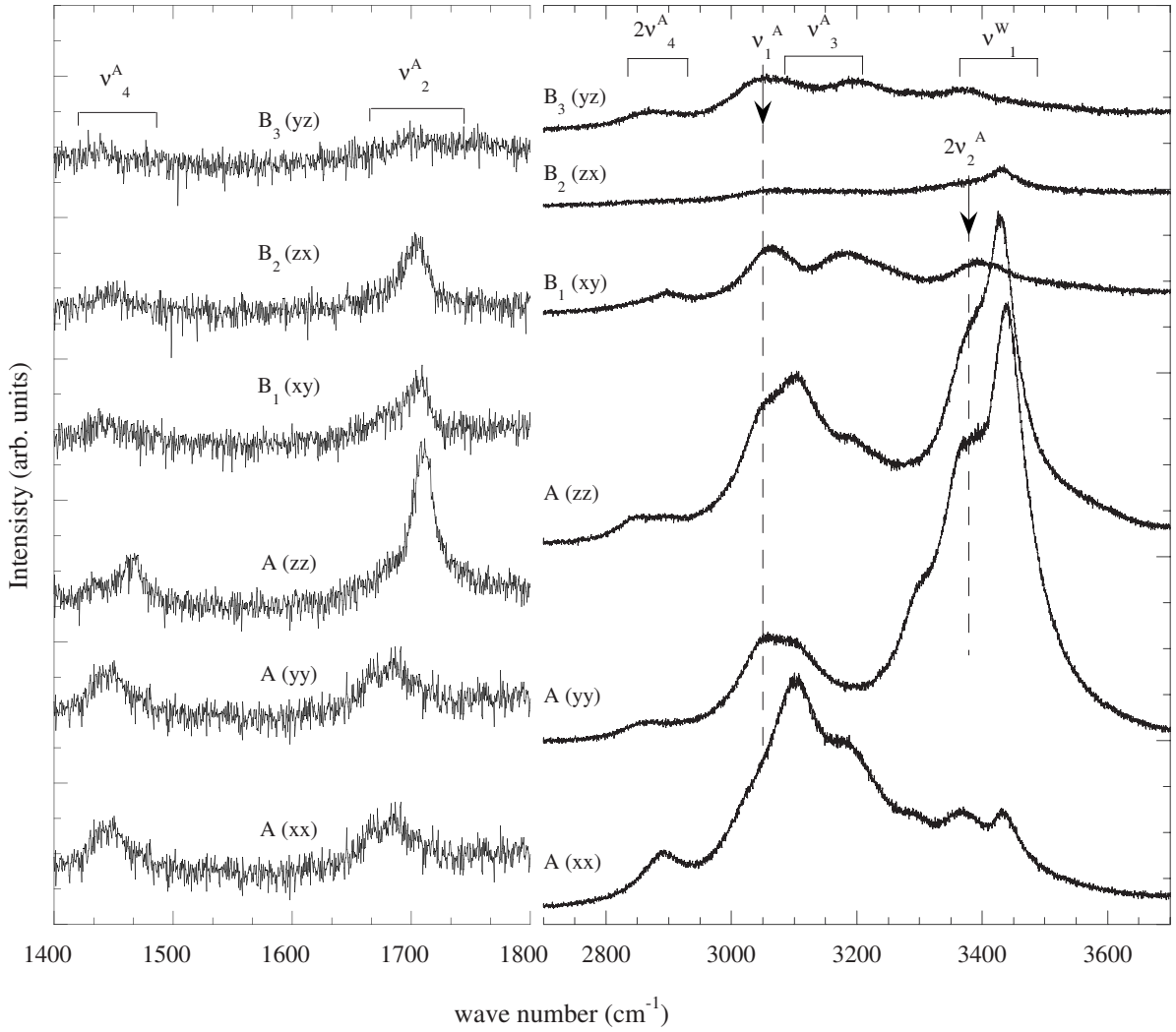

FIG. 4. Raman spectra of SASD recorded at room temperature for six scattering geometries in the wave number range of internal vibration of the ammonium ion and water molecules. The spectra are vertically shifted by comparison.

dence for a strong anharmonicity of ammonium ion vibrations, even in the paraelectric phase.

Table II summarizes the mode assignments reported in this work at room temperature.

B. Temperature dependence of the spectra

As was referred to above, the crystal structure of the ferroelectric phase of SASD is unknown. The study of some features regarding the low temperature phase transitions in SASD will be achieved by analyzing the *A* and some *B* spectra as a function of the sample temperature.

While the Raman spectra of SASD present sudden changes in the vicinity of $T_{c1}=100$ K, around $T_{c2}=80$ K they follow a smoother temperature variation. Moreover, we also observe the appearance of very weak, but well defined, Raman bands below $T_{c2}=80$ K. The discrepancy between the value of T_{c2} found in this work and the one reported in the current literature[8] may be due to the crystal preparation conditions.

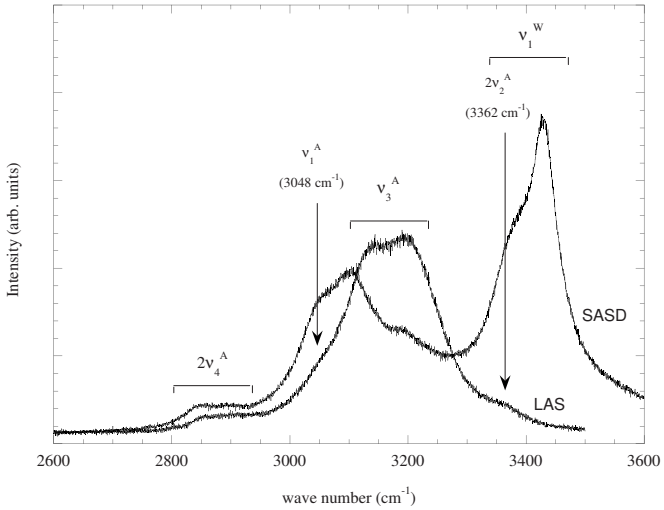

FIG. 5. Raman spectra of SASD and LAS in the wave number range of internal vibration of the ammonium ion and water molecule.

TABLE II. Wave number (in cm^{-1}) of some Raman bands observed in SASD single crystal at room temperature.

Wave number (cm^{-1}) and species	Assignment
262, 380 $A(xx)$	ν_6^A
261, 377 $A(yy)$	
263, 374 $A(zz)$	
263 B_1	
452, 460 $A(xx)$	ν_2^S
452, 460 $A(yy)$	
453 $A(zz)$	
457 B_1	
455 B_2	
454 B_3	
584 $A(xx)$	Water libration
506, 583 $A(yy)$	
506 $A(zz)$	
587 B_3	
616, 625 $A(xx)$	ν_4^S
617, 625 $A(yy)$	
624 $A(zz)$	
596, 623 B_1	
600, 620 B_2	
624 B_3	
906 $A(xx,yy,zz)$	$2\nu_2^S$
986 A, B_1, B_2, B_3	ν_1^S
1067 $A(xx)$	ν_{3a}^S
1066 $A(yy)$	
1064 $A(zz)$	
1065 B_2	
1105 $A(xx)$	ν_{3b}^S
1107 $A(yy)$	
1106 $A(zz)$	
1130 $A(xx,zz)$	ν_{3c}^S
1132 $A(yy)$	
1135 B_1	
1133 B_2	
1134 B_3	
1445 $A(xx,yy)$	ν_4^A
1432, 1466 $A(zz)$	
1443 B_1	
1448 B_2	
1667, 1687 $A(xx,yy)$	ν_2^A
1679, 1781 $A(zz)$	
1676, 1709 B_1	
1704 B_2	
1669 B_3	
2892 $A(xx)$	$2\nu_4^A$
2868 $A(yy)$	
2847, 2895 $A(zz)$	
2898 B_1	
3048 A, B_2, B_3	ν_1^A
3105, 3183 $A(xx)$	ν_3^A
3099 $A(yy)$	
3099, 3190 $A(zz)$	
3183, 3228 B_1	
3378 $A(xx,zz)$	$2\nu_2^A$, ν_1^W
3369 $A(yy)$	
3370 B_3	
3438 $A(xx)$	ν_1^W
3432 $A(yy)$	
3429 $A(zz)$	
3423 B_1	
3432 B_2	
3432 B_3	
3519 $A(yy)$	ν_3^W

In the following, we present the temperature dependence of the Raman spectra, registered between 10 and 300 K, as well as the temperature dependence of the vibrational parameters, determined using the fitting procedure mentioned above.

1. Lattice modes

Figure 6 shows the low frequency Raman spectra of SASD, recorded at different fixed temperatures in the $y(XX)z$, $x(YY)z$, and $y(XY)z$ scattering geometries. The temperature dependence of the corresponding wave number is depicted in Fig. 7. The insets of Fig. 7 show the temperature dependence of the damping coefficient of some selected lattice modes.

In general, as the temperature decreases from 300 K, the lattice modes tend to harden and their damping coefficient decreases as a result of anharmonic effects and thermal changes. Neither a soft mode nor any relaxational mode was found by the quantitative analysis of the low frequency spectra.

Near $T_{c1}=100$ K, we observe a sudden change of the spectra associated with the appearance of new bands and the abrupt change of intensity of some existing bands. The temperature dependence of both the wave number and the damping coefficient of almost all visible lattice modes show an anomalous behavior in the neighborhood of $T_{c1}=100$ K. The damping factor as a function of the temperature presents a cusplike anomaly at T_{c1} for various modes, some of which

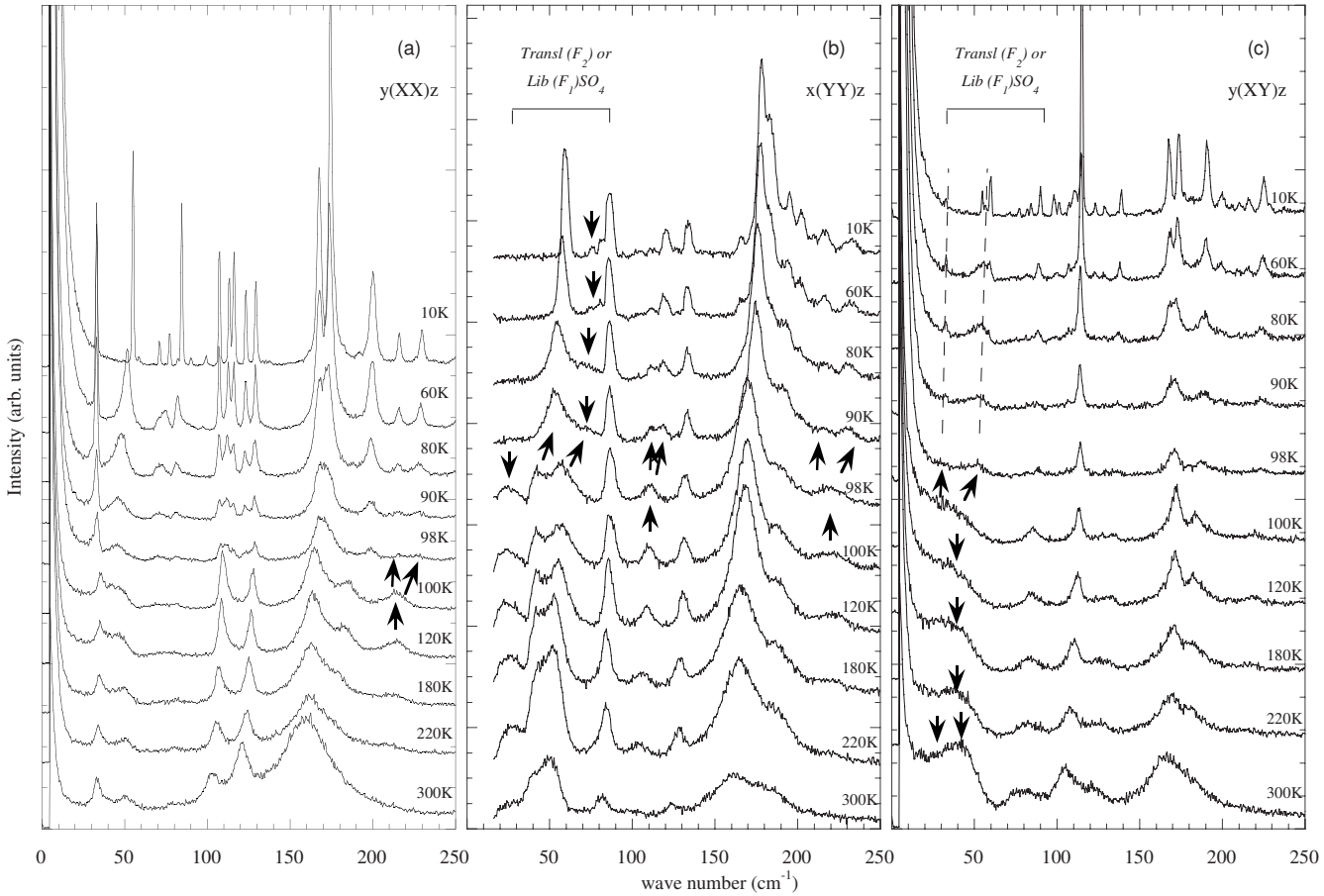

FIG. 6. Temperature dependence of the Raman spectra in the wave number range of external modes. From left to right: (a) $y(XX)z$, (b) $x(YY)z$ and (c) $y(XY)z$ scattering geometries.

are associated with the lattice translations and librations of the ammonium ion. For example, the band visible at 262 cm^{-1} (room temperature value) in the $x(YY)z$ spectra splits into two components, while its damping factor shows a peak at T_{c1} (see inset of Fig. 7(b)). This band has been assigned to the external libration on the NH_4^+ ion (ν_6^A). Another example in the same scattering geometry is observed in the temperature dependence of the wave number and damping factor of the band located at 186 cm^{-1} (room temperature value), which corresponds to translations of the ammonium ion. In this case, while the wave number shows a small but clear anomaly at 98 K, the damping coefficient presents a divergence at T_{c1}. Finally, the band located at 102 cm^{-1} (room temperature value) in the $x(YY)z$ spectra splits into two bands at T_{c1}.

An interesting result is obtained by analyzing the complex temperature evolution of the low wave number range of the $x(YY)z$ and $y(XY)z$ spectra, in the vicinity of the first phase transition at $T_{c1}=100$ K [see Figs. 6(b) and 6(c)]. In the $x(YY)z$ spectra, we observe an abrupt upward shift of the wave number of the bands located at 43 and 52 cm^{-1} (values at room temperature), respectively, at T_{c1}. The intensity of the band at 52 cm^{-1} decreases abruptly below T_{c1}. The damping coefficient of the band located at 52 cm^{-1} (room temperature value) presents interesting temperature dependence. In fact, the damping coefficient increases monotonically as the temperature decreases toward T_{c1}, where it displays a maximum value, and then decreases with decreasing temperature. A similar behavior is found in the temperature dependence of the damping factor of the lowest wave number mode observed in the $y(XX)z$ Raman spectra [see Fig. 7(a)].

The abrupt shift and the decrease of the intensity of lattice bands below T_{c1} are also found in the $y(XY)z$ spectra. The broad bands located at 34 and at 44 cm^{-1} (room temperature values) observed in the $y(XY)z$ spectra soften as the temperature decreases down to T_{c1}, and just below that temperature, the wave number of the upper frequency band shifts upward to 50 cm^{-1}, while the wave number of the lowest frequency band remains practically constant. Simultaneously, we observe an abrupt decrease of the intensity of these bands.

The second phase transition, occurring in our samples at $T_{c2}=80$ K, manifests itself as small anomalies in the temperature dependence of the wave number of some lattice modes and by the appearance of new weak bands below $T_{c2}=80$ K [see Figs. 7(a) and 7(b)].

2. SO_4^{2-} *internal modes and water librations*

The relevant information regarding the temperature behavior of the internal modes of the sulphate ion is better obtained by analyzing the temperature evolution of the $x(ZZ)y$ Raman spectra. Figure 8 shows the $x(ZZ)y$ Raman

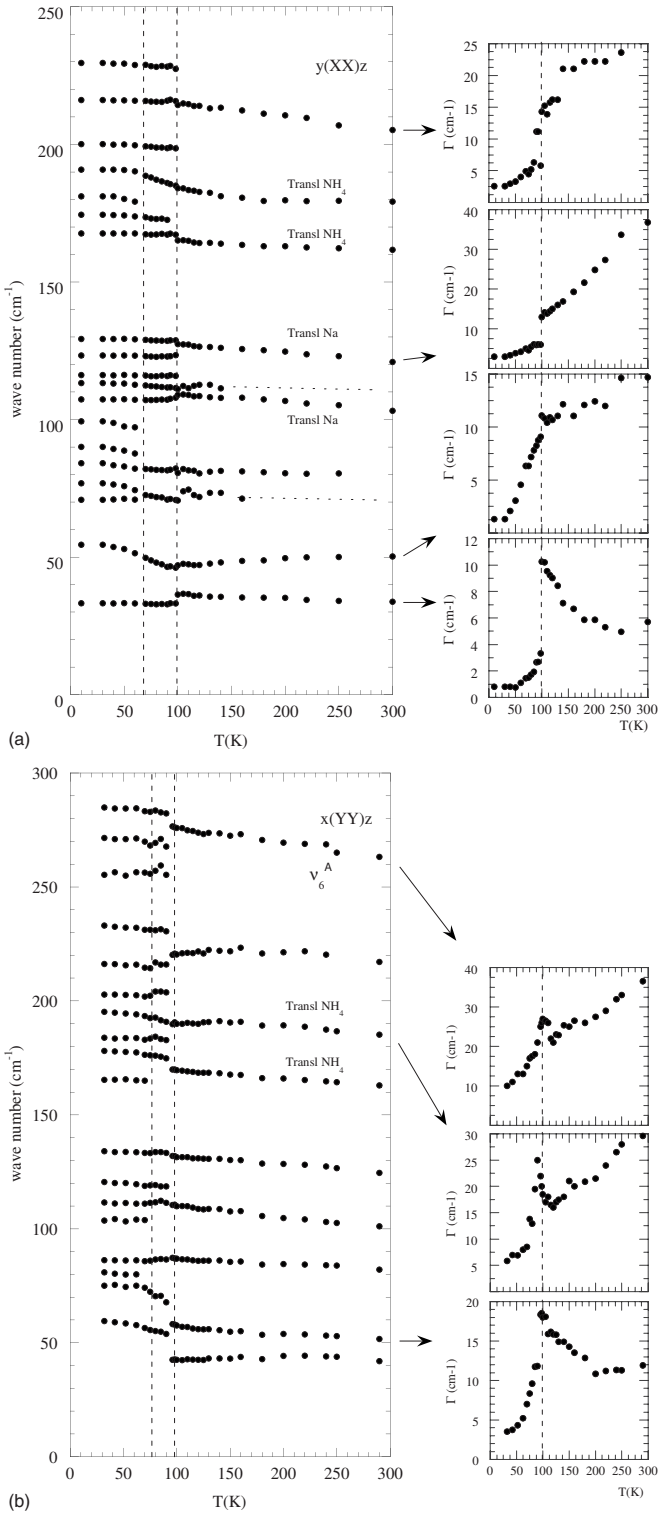

FIG. 7. Temperature dependence of the wave number of the external modes observed in the (a) $y(XX)z$ and (b) $x(YY)z$ scattering geometries. Insets: Temperature dependence of the damping coefficient of some selected modes. The vertical dashed lines indicate the critical temperatures.

spectra at different fixed temperatures in the wave number range where the internal modes of the sulphate ion can be observed. Figure 9 shows the temperature dependence of both the wave number and the damping factor of some selected internal modes observed in the 300–1200 cm^{-1} spectral range. As can be seen, the ν_2^S mode presents anomalous behavior (with regard to the temperature dependence) of its wave number near T_{c1}. However, no evidence of critical features in the vicinity of $T_{c2}=80$ K can be detected. The damping factors associated with the ν_{2a}^S and the ν_{2b}^S show, respectively, a cusplike and a steplike anomaly at $T_{c1}=100$ K. The temperature dependence of the wave number of the ν_4^S mode presents a small anomaly near T_{c1}, but not at T_{c2}. Interesting behavior is displayed by the water libration modes. As the temperature is lowered, the wave number of the lower component increases, while the higher frequency component remains practically temperature independent. At T_{c1}, each of the two bands associated with the water libration modes splits abruptly. We observe that the wave number difference between the two components, resulting from the splitting of the lower wave number band, is about 45 cm^{-1} at T_{c1}. The weak band located at 608 cm^{-1} (value at 140 K), clearly visible below 150 K, is not resolved above this temperature and, consequently, it cannot be fitted above 150 K. The existence of this band is signalized with the dashed line in Fig. 9(a). This band is no longer detectable below T_{c1}. The ν_6^A mode hardens as the temperature is lowered from 300 K toward T_{c1}. The wave number as a function of the temperature shows an upward jump at T_{c1} and, for further cooling, no anomalous behavior is found. The damping coefficient of the ν_6^A mode displays a downward jump at T_{c1}.

Concerning the stretching modes of the sulphate ion, we observe an abrupt downward jump of the wave number as a function of the temperature of the ν_{3b}^S mode at $T_{c1}=100$ K, whereas the temperature dependence of the wave number of the ν_{3a}^S mode displays a continuous variation across the phase transition. In Fig. 9(b), a splitting of the ν_{3c}^S band is clearly observed. As there are two nonequivalent sites below T_{c1}, a splitting of the ν_1^S band is also expected, but there is no experimental evidence for this occurrence. We have tried to fit this band with two oscillators, but the difference between the frequencies of each mode is about 2 cm^{-1}, which is within the experimental error. The damping coefficient (as a function of the temperature) of the stretching modes shows critical behavior around T_{c1}, some of them showing a peak. New weak bands mark the onset of the second phase transition at $T_{c2}=80$ K.

3. NH_4^+ *internal modes and water stretching modes*

Figure 10 shows the Raman spectra of SASD in the spectral range of the bending and stretching modes of the ammonium ion, recorded at various temperatures in the $x(ZZ)y$ scattering geometry. Figure 11 shows the temperature dependence of the wave number and the damping factor of some selected modes shown in Fig. 10.

The ν_2^A and ν_4^A modes are well separated from the remaining modes, so their assignment is straightforward. As we can see in Fig. 11(a), the wave number of the bending modes ν_2^A of the ammonium ion shows a linear increase as the temperature is lowered toward T_{c1}. However, below $T_{c1}=100$ K, the wave number remains practically independent of the temperature. The dashed lines in Fig. 11(a) are qualitative ex-

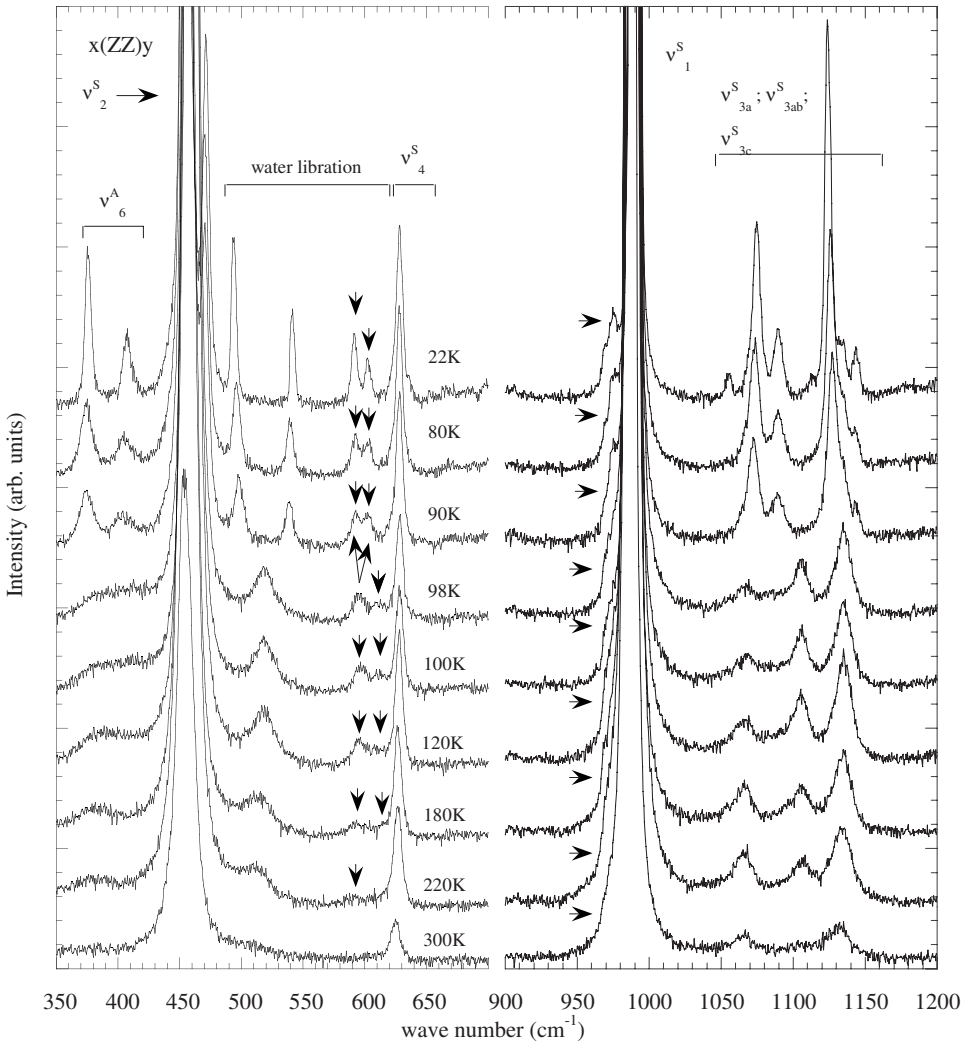

FIG. 8. The $x(ZZ)y$ Raman spectra in the wave number range of internal modes of the sulphate ion for different temperatures, between 10 and 300 K.

trapolations, for $T<T_{c1}$, of the temperature behavior observed in the paraelectric phase. It can be seen that the experimental data are shifted downward relative to the corresponding dashed line. As the ammonium ions are attached to sulphate anions by hydrogen bonds, forming NH_4^+-SO_4^{2-}-NH_4^+ chains, this result may be interpreted as a consequence of proton ordering along the N-H-O hydrogen bonds.[22] In fact, if the protons become ordered, each of them attaches itself to one tetrahedral unit, resulting in a more massive unit, which causes the lowering of its frequency. The temperature dependence of the ν_2^A at T_{c1} agrees quite well with this prediction. Moreover, the damping factor of each of the ν_2^A modes shows different temperature dependences. The damping coefficient of the lower frequency ν_2^A mode displays a maximum value near 150 K and a sudden decrease at T_{c1}. The temperature dependence of the damping coefficient of the ν_2^A component with higher frequency displays a small cusplike anomaly at T_{c1}. Concerning the ν_4^A modes, we observe a clear anomaly in the temperature dependence of the wave number at T_{c1}. The damping factor of the lower frequency component shows a maximum value in the vicinity of 150 K and a small peak at T_{c1}, followed by a sudden decrease below that temperature. In this spectral range, we detect a new band below T_{c1} (1440 cm^{-1} at T_{c1} = 100 K).

The ν_1^A and ν_3^A modes are located at higher frequencies. In the 2800 and 3500 cm^{-1} spectral range, there are a strong mode mixing and an overlap of different modes and overtones. Figure 11(b) shows the temperature dependence of the wave number and the damping factor of some selected modes in the 2800 and 3500 cm^{-1} spectral range. As illustrated in Fig. 11(b), the wave number of the ν_1^A mode shows a temperature independent behavior from room temperature to 120 K. Below 150 K, the wave number increases slightly. At T_{c1}, both the wave number and the damping factor of the ν_1^A mode depict a jump. The damping coefficient of the ν_1^A mode displays small anomalies near 200 K and at T_{c1} = 100 K. The ν_3^A modes exhibit definite, but small changes in wave number at T_{c1}. Their damping factors display a steplike behavior near 200 K and at T_{c1} = 100 K.

The water stretching modes give rise to broad bands at room temperature. Definite steplike anomalies are visible at

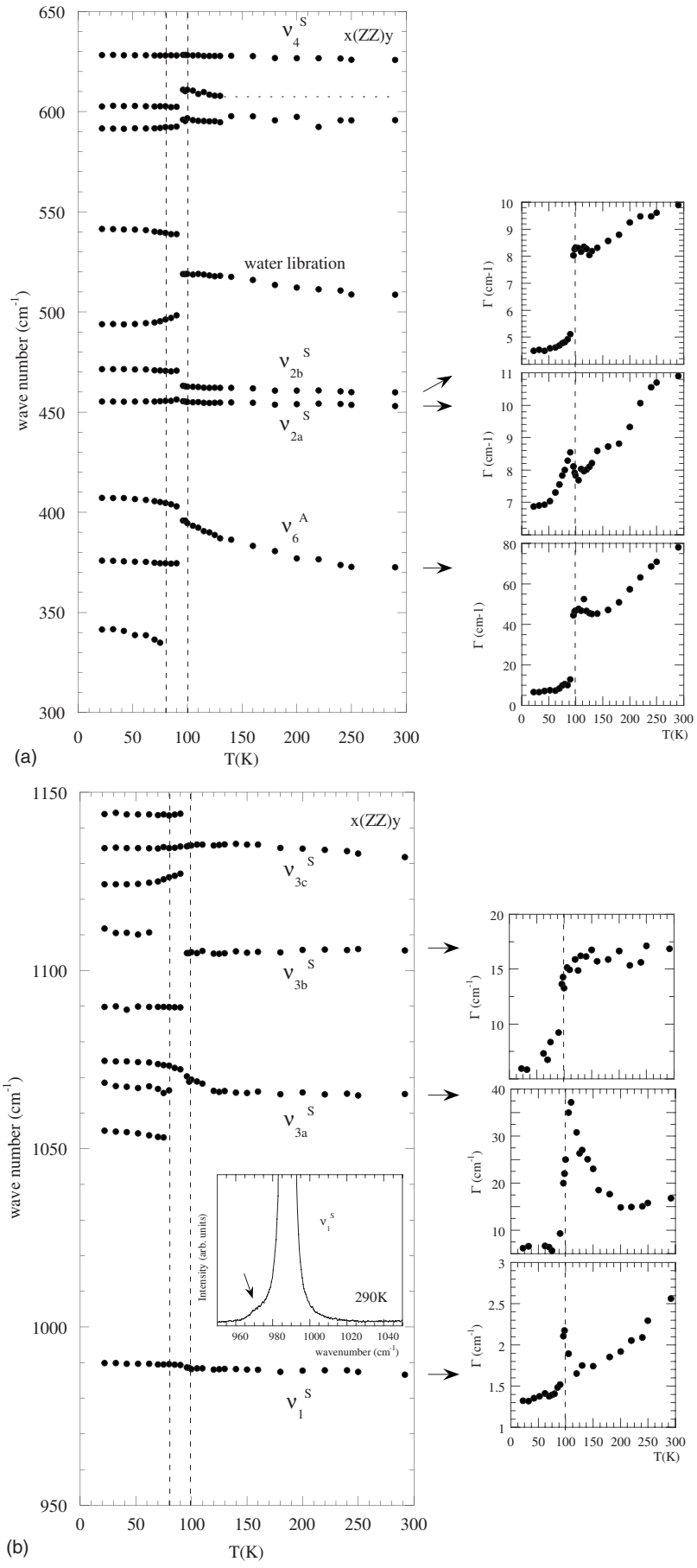

FIG. 9. Temperature dependence of the wave number of the internal modes observed in the frequency range of the sulphate ion internal vibrations, observed in $x(ZZ)y$ scattering geometries. Insets: Temperature dependence of the damping coefficient of some selected modes. The vertical dashed lines indicate the critical temperatures. The horizontal dashed line indicates the wave number of the mode obtained by visual observation of the spectra.

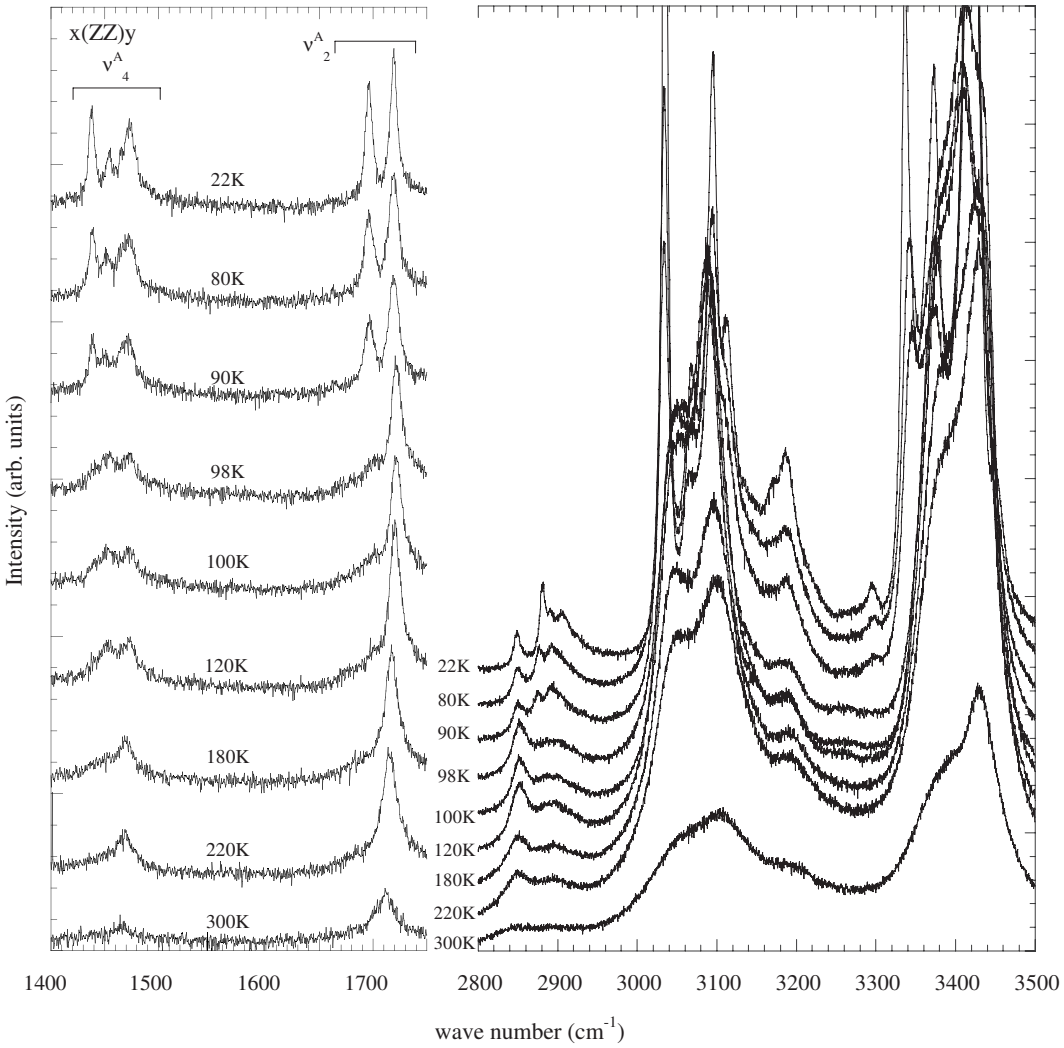

FIG. 10. The $x(ZZ)y$ Raman spectra in the wave number range of internal modes of the ammonium ion and stretching vibrations of the water molecule for different temperatures, between 10 and 300 K.

T_{c1} in the temperature dependence of the wave number. The damping coefficients of the stretching modes display a complex thermal behavior. Our results reveal a change in the temperature derivative of the damping factor ($d\Gamma/dT$) near 190 K. The phase transition at T_{c1} manifests itself by pronounced anomalies in the temperature dependence of the damping factor. Another anomaly in $d\Gamma/dT$ is detected at around 80 K. New bands mark the phase transition at $T_{c1}=100$ K and at $T_{c2}=80$ K.

C. Discussion and conclusions

The data reported in this work have shown that the temperature dependence of the wave number and of the damping factor of most vibrational modes have appreciable alterations in the vicinity of the ferroelectric phase transition at $T_{c1}=100$ K. The changes in the temperature behavior of some internal modes associated with the ammonium ion and with the water molecule undoubtedly reveal the existence of structural modifications that occur at 200 K and at 150 K, corresponding mainly to their deformations and, in particular, for water molecules. This result may indicate the existence of precursory deformations or reorientations of the molecular units above the phase transition temperature, which take place between 150 and 200 K. In addition, the appearance of new bands below $T_{c2}=80$ K also gives evidence of a new phase transition at this temperature, accompanied by a symmetry breakdown.

In the paraelectric phase of SASD, all modes are nondegenerate and, consequently, the splitting observed in their bands at $T_{c1}=100$ K is interpreted as a result of deformations in molecular units, which become nonequivalent in the unit cell of the ferroelectric phases. This type of behavior is clearly observed in some modes involving sulphate and ammonium ions and water molecule vibrations.

The current literature reports that the SO_4^{2-} and SeO_4^{2-} groups contribute predominantly to the phase transitions of SASD and SASeD, respectively.[12] In the paraelectric phase, the two sublattices of SO_4^{2-} (I) and SO_4^{2-} (II) are equivalent but oppositely oriented so that the total polarization of each unit cell is zero. Below T_{c1}, due to different angles at which the active groups turn, the symmetry of the crystal lowers [$P2_1$ or $P1$ (Ref. 23)] and a nonzero polarization appears. For a rigorous treatment of the interaction between these two

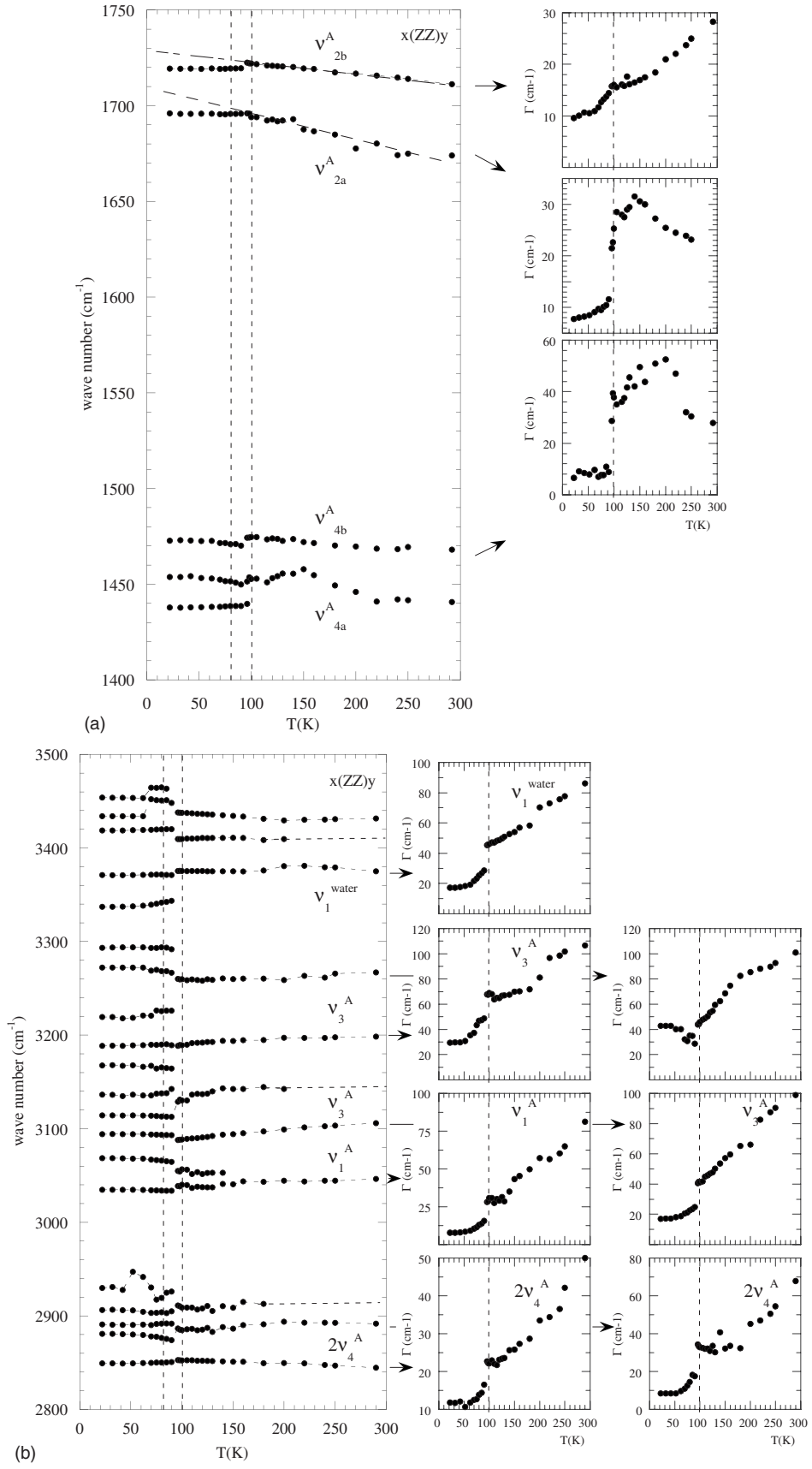

FIG. 11. Temperature dependence of the wave number of the internal modes observed in the frequency range of the ammonium ion internal vibrations, observed in $x(ZZ)y$ scattering geometries. Insets: Temperature dependence of the damping coefficient of some selected modes. The horizontal dashed lines indicate the wave number of the mode obtained by visual observation of the spectra.

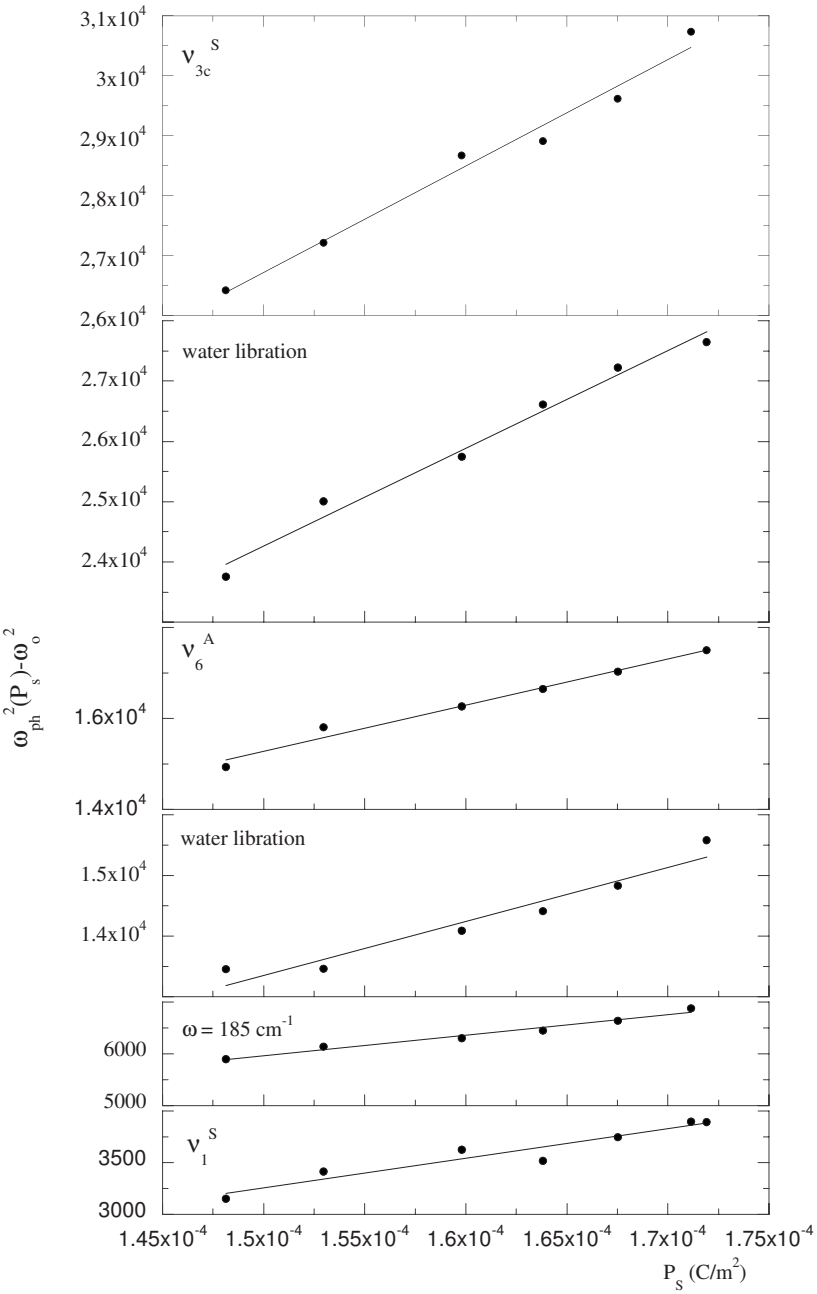

FIG. 12. Square wave number difference $(\omega_{ph}^2-\omega_o^2)$ of some external and internal modes as a function of the spontaneous polarization, where ω_o was calculated by extrapolating the linear behavior of $\omega_{ph}(P_S)$ to the $P_S=0$ value.

active groups, SO_4^{2-} (I) and SO_4^{2-} (II) identified with pseudospins, a modified Mitsui Hamiltonian was proposed.[12] A good correlation between the dielectric susceptibility calculated with this model and the corresponding experimental data has been found.[12]

The analysis of the Raman spectra also provides evidence for proton ordering in the NH_4^+-SO_4^{2-}-NH_4^+ chains of SASD at the phase transition at T_{c1}. In fact, we have observed an abrupt shift of the wave number of some modes related to sulphate and ammonium ions as well as a steep decrease in the intensity of some bands associated with lattice modes in the paraelectric-ferroelectric phase transition. The frequency shift observed is due to a change of the intermolecular interaction caused by a proton ordering, and the abrupt decrease of the intensity is due to a new orientation of the molecular units. When a molecular unit changes the spatial orientation of its inertia principal axis, the Raman tensor elements alter in the primitive referential, inducing changes in the intensity of the associated bands. Therefore, the new orientation of sulphate ions can increase the length of the hydrogen bonds in the NH_4^+-SO_4^{2-}-NH_4^+ chains, and consequently, proton ordering may take place.

On the basis of magnetic resonance data, it was proposed that the phase transition of SASD at $T_{c1}=100$ K is of displacive nature with relatively large lattice distortions,[23] but no clear evidence for an optical soft mode is reported in the available literature. In the work here reported, no evidence was found for an optical soft mode in the Brillouin zone center. Also, no relaxational mode was detected in the low frequency Raman spectra and is in good agreement with the results previously reported by Ribeiro *et al.*[7] The critical behavior observed in the dielectric constant as a function of the

temperature, along the c axis, is entirely due to excitations with typical frequencies that are much lower than the phonon frequencies observed.

Some aspects of the observed critical behavior of the normal modes can be described by considering a model that accounts for the coupling between pseudospins and the normal coordinates of the lattice modes and the internal vibrations. We shall assume that the Hamiltonian of SASD is given by

$$H = H_L + H_s + H_{L,S}, \tag{2}$$

where H_L is the harmonic lattice Hamiltonian,[4] H_S is the Mitsui pseudospin Hamiltonian,[12] and $H_{L,S}$ is the term describing the interaction between phonons and pseudospins. This last term is expressed as a power expansion of the type[4]

$$H_{S,L} = H_{S,L}^{(1)} + \sum_{\vec{k},\vec{k}'} V(\vec{k},\vec{k}')Q(\vec{k})Q^*(\vec{k}+\vec{k}')S(\vec{k}') + \sum_{\vec{k},\vec{k}',\vec{k}''} W(\vec{k},\vec{k}',\vec{k}'')Q(\vec{k})Q^*(\vec{k}+\vec{k}'+\vec{k}'')S(\vec{k}')S(\vec{k}'') + \cdots . \tag{3}$$

Here, $H_{S,L}^{(1)}$ represents a bilinear pseudospin-phonon interaction, $Q(\vec{k})$ is the normal coordinate of a given normal mode with the wave vector $\vec{k}$, $V(\vec{k},\vec{k}')$ and $W(\vec{k},\vec{k}',\vec{k}'')$ are coupling constants, and $S(\vec{k})$ is the Fourier transform of the z projection of the pseudospin operator.

Retaining only the first term of the expansion (3), no frequency shift of optical phonons is found because the Hamiltonian can be transformed by eliminating the interaction term into a displaced oscillator at the unperturbed phonon frequency. So, in order to account for anomalies, we need to consider terms that are at least quadratic in the normal mode coordinates.

The second- and lower-order terms in Eq. (3) account approximately for the frequency anomalies. The effect of these terms is the renormalization of the phonon frequencies which, for $\vec{k}'=\vec{0}$ and after replacing $S(\vec{0})$ by its thermal average $\langle S(\vec{0})\rangle$, is expressed as follows:

$$\omega_{ph}^2(T,\vec{k}) = \omega_0^2 + 2V(\vec{k})\langle S(\vec{0})\rangle. \tag{4}$$

By assuming that the electric polarization is proportional to the mean value of $S(\vec{0})$, the shift of the square of the phonon frequency is proportional to the spontaneous polarization $P_S(T)$. $P_S(T)$ data were calculated by an integration of the pyroelectric current. An extrapolation procedure enables us to calculate the spontaneous polarization at the same Raman spectra recording temperatures.

Figure 12 shows the polarization dependence of the square of the wave number for some lattice and internal modes of SASD. The bands depicted in Fig. 12 correspond to the $x(YY)z$ Raman modes detected at 185 cm^{-1} (translation of NH_4^+) and 372 cm^{-1} (ν_6^A), water librations, and symmetric (ν_1^S) and asymmetric stretching (ν_{3c}^S) modes of sulphate ion (see Figs. 7 and 9). In agreement with the behavior predicted by Eq. (4), a linear dependence on polarization of the square of the frequency for the lattice and the internal modes referred above can be seen in Fig. 12. The slope of the lines is proportional to the coupling coefficient $V(\vec{k})$ between normal modes and pseudospins. As expected, we can see that the coupling coefficient is different for the different modes. Among the lattice and internal modes, the stronger coupling occurs between the pseudospins and the asymmetric stretching mode of the sulphate ion, whereas the weakest one occurs between the pseudospins and the symmetric stretching mode of the same ion. This result can be interpreted straightforwardly by taking into account the polar character of the internal modes. In fact, as the symmetric stretching mode is a weak polar mode, the coupling between the polar pseudospins and this mode is expected to be small. On the other hand, due to the polar character of the sulphate ion asymmetric stretching mode, the coupling between pseudospins and that mode is expected to be the strongest.

*jamoreir@fc.up.pt

[1] R. A. Cowley, Adv. Phys. **29**, 1 (1980).
[2] R. M. Hill and S. K. Ichiki, Phys. Rev. **132**, 1603 (1963).
[3] D. Merunka and B. Pakvin, Solid State Commun. **129**, 375 (2004).
[4] G. Schaack and V. Winterfeldt, Ferroelectrics **15**, 35 (1977).
[5] J. A. Moreira, A. Almeida, L. G. Vieira, J. L. Ribeiro, M. R. Chaves, M. L. Santos, and A. Klöpperpieper, Phys. Rev. B **72**, 094111 (2005).
[6] E. Corozza and C. Sabelli, Acta Crystallogr. **22**, 683 (1967).
[7] J. L. Ribeiro, L. G. Vieira, I. Tarroso Gomes, J. Agostinho Moreira, A. Almeida, M. R. Chaves, M. L. Santos, and P. P. Alferes, J. Phys.: Condens. Matter **18**, 7761 (2006).
[8] Y. Makita and T. Sekido, J. Phys. Soc. Jpn. **20**, 954 (1965).
[9] I. E. Lipinski, J. Kuriata, I. Natkaniec, and A. Pawlukojc, Phys. Status Solidi B **227**, 477 (2001).
[10] N. A. Korynevskii, Ferroelectrics **268**, 207 (2000).
[11] I. E. Lipinski, N. A. Korynevskii, J. Kuriata, and W. Pastusiak, Physica B **327**, 116 (2003).
[12] I. E. Lipinski, J. Kuriata, and N. A. Korynevskii, Ferroelectrics **317**, 115 (2005).
[13] V. Fawcett, D. A. Long, and V. N. Sankaranayanan, J. Raman Spectrosc. **3**, 197 (1975).
[14] V. Fawcett, D. A. Long, and V. N. Sankaranayanan, J. Raman Spectrosc. **3**, 217 (1975).
[15] Yu Y. Yuzyuk, V. I. Torgashev, and A. H. Fuith, J. Phys.: Condens. Matter **11**, 889 (1999).
[16] B. H. Torrie, C. C. Lin, O. S. Binbrek, and A. Anderson, J. Phys. Chem. Solids **33**, 697 (1972).
[17] E. L. Wagner and D. E. Horning, J. Chem. Phys. **18**, 305 (1950).
[18] P. K. Acharya and P. S. Naraynan, Indian J. Pure Appl. Phys. **11**, 514 (1973).

[19] G. Herzberg, *The Infrared and Raman Spectra of Polyatomic Molecules* (Van Nostrand, New York, 1945).
[20] K. Nakamoto, *Infrared Spectra of Inorganic and Coordination Compounds*, 4th ed. (Wiley, New York, 1962).
[21] G. Turrel, *Infrared and Raman Spectra of Crystals* (Academic, London, 1972).
[22] E. Courtens and H. Vogt, J. Chem. Physique **82**, 317 (1985).
[23] D. J. Genin and D. E. O'Reiley, J. Chem. Phys. **50**, 2842 (1969).